

## RESEARCH ARTICLE

# An Improvement in Dynamic Behavior of Single Phase PM Brushless DC Motor Using Deep Neural Network and Mixture of Experts

YANG ZHANG<sup>1</sup>, RADOMIR GONO<sup>2</sup>, (Senior Member, IEEE),  
AND MICHAŁ JASIŃSKI<sup>2,3</sup>, (Member, IEEE)

<sup>1</sup>Beijing Aiqi Technology Company Ltd., Beijing 100089, China

<sup>2</sup>Department of Electrical Power Engineering, Faculty of Electrical Engineering and Computer Science, VSB—Technical University of Ostrava, 708 00 Ostrava, Czech Republic

<sup>3</sup>Department of Electrical Engineering Fundamentals, Faculty of Electrical Engineering, Wrocław University of Science and Technology, 50-370 Wrocław, Poland

Corresponding author: Radomir Gono (radomir.gono@vsb.cz)

This work was supported by the VSB—Technical University of Ostrava under SGS Grant SP2023/005.


**ABSTRACT** Brushless DC motors play a vital role as a workhorse in many applications, especially home appliances. In the competitive world of the day, a brushless DC motor is a wise choice for many applications because of its high power density, a simple driving circuit, and high efficiency. Accordingly, demonstrating the feasibility of a new controller on this type of motor has undoubtedly paramount importance. Two methods of speed controllers, namely linear-quadratic regulator, and proportional-integral-derivative, are mixed using a mixture of experts (MoE) for a single-phase PM brushless DC external rotor motor. The dynamic model of the SP PM BLDC ER motor characterizes the behavior of the motor, involving cogging torque and electromotive force (EMF) gained from 2D finite element analyses. The motor is supplied by a pulse width modulation inverter with a constant voltage source. The results disclose that the SP PM BLDC performance is enhanced and more robust during load disturbance. ANSYS and MATLAB environments are used for obtaining finite element analysis and dynamic analysis of single-phase PM brushless DC external rotor motors, respectively. The merits of the proposed approach are validated through implementing a low-scale experimental setup.

**INDEX TERMS** Brushless DC motor, controlling system, finite element, power electronic converter.

## I. INTRODUCTION

External rotor motors are exceedingly utilized in high power density applications such as automotive, aerospace, home appliances, etc., owing to their inherent ability to transmit torque from their outer sides [1], [2], [3]. Coupled with the feature above, widespread attention has been paid to the brushless direct current (BLDC) motors providing higher efficiency at the higher speed [4], [5]. This originates from the fact that the BLDC motors employ the electrical commutating mechanism in comparison with the extensively used universal motors in which a mechanical mechanism is in charge of supplying power to the windings. Since the BLDC motors

are permanent magnet motors where solid-state switches control the commutation, they have met maintenance requirements [6], [7]. These features have made the BLDC motors a potential workhorse in the home appliances industry [8]. Single-phase BLDC motors can provide a suitable torque in the lower weight, smaller size, and more simple structure in comparison with three-phase BLDC motors [9], [10]. Therefore, single-phase permanent magnet brushless DC external rotor (SP PM BLDC ER) motors are used as low horse-power machines. SP PM BLDC ER motor has a permanent magnet on its rotor placed on the outer part of the motor and the windings on the stator, which are commutated electronically. SP PM BLDC ER motor is cost-effective and effortless to mass production compared to single-phase induction machine [11]. SP PM BLDC ER motor is not

The associate editor coordinating the review of this manuscript and approving it for publication was Amin Mahmoudi .

self-starting; hence this type of machine has been designed so that there is another torque acting in addition to excitation torque confirmed by the interaction between stator winding current and permanent magnet field. Thus machine designers contrive an asymmetric air gap to establish cogging torque, which originated from the fact that the stator tooth and PM field are interacted [12], [13], [14].

In the single-phase BLDC high-speed motors, three diverse controlling methods, including commutation pulse [15], phase advance [16], and reference voltage-controlled pulse width modulation [5], [17] have been extensively used. A digital controller such as a microcontroller or microprocessor has been employed for implementing the commutation pulse or phase advance controls or a combination thereof in which a sequence of the input voltage is sensed [18]. Although the ability of SP PM BLDC motor performance in the variable input voltage and variable load torque can be achieved without pulse amplitude modulation or pulse width modulation (PWM) in the hybrid control (combination of commutation pulse and phase advance), they are not able to reduce the excitation torque ripple. Thus the idea of reference voltage-controlled PWM was bounced around to reduce torque ripple [19], [20]. The controller uses PWM high-frequency signals for deteriorating the undesirable current ripple in the high-speed operation while the reference voltage is linearly decreasing rather than shifting the input voltage phase. However, its higher switching frequency leads to lower efficiency in high-speed applications.

In addition to the torque ripple reduction, the electrical and mechanical response performance of the SP PM BLDC ER motors is of paramount. The ability of accelerated response to load and input voltage of the motor has gained lots of attention in recent years [7], [21], [22]. In this regard, several types of high-level controlling algorithms, such as adaptive, conventional proportional-integral-derivative (PID), nonlinear, fuzzy, and discrete controllers, have been implemented in BLDC motor drives [23], [24], [25].

Guo et al. [26] have proposed a new adaptive integral sliding mode (SM) controller for BLDC motors to mitigate related problems of speed fluctuation overload torque disturbance. A Kalman-based load disturbance observer set up, and an adaptive saturation function is applied to the error link to lessen the windup phenomenon [27]. Then, the convergence and stability of the controller are investigated through the Lyapunov method. Although this controller damped the BLDC torque under fast loading variations, its implementation is to somewhat complicated. A novel 2<sup>nd</sup> order sliding mode coupled with the super-twisting algorithm is presented in [28] for BLDC motor drivers. The proposed method is capable of properly dealing by the uncertainties and load disturbance with using a super-twisting method. The necessity of using current and voltage control loops or any complicated reference frame transformations demolished in the introduced process. The main detriments of the traditional sliding mode controller, including chattering effects

and high-frequency switching, are relieved at the expense of the torque ripple increase when the external disturbances are applied.

A fuzzy neural network (FNN) controlling scheme is proposed and implemented in [29] for BLDC motor drives. As reported, the sole employing of the fuzzy logic controller has posed two significant problems, including poor rough granulation and non-adaptation and harrowing extraction and adjustment of fuzzy roles. The idea of the proposed FNN is to characterize the fuzzy rules based on a trainable algorithm, such as a neural network [29]. The results seem reasonable while using an extended Kalman filter training algorithm. The proposed FNN provides the capability for adaptive self-tuning of the weights and memberships of the input parameters for fuzzy logic. Sedaghati et al. [30] proposed a novel type-2 fuzzy controlling scheme based on the adaptive immersion and invariance (I&I) control method for speed controlling of the BLDC motors. The mathematical model parameters and their associated uncertainties contemplate as unknown parameters. The approximation error is tracked with the proposed fuzzy compensator, and its corresponding rule parameters are tuned using the Lyapunov stability method. The performance of the proposed method is investigated during the disturbance of load torque and stator coil resistance. The results reveal that although the performance of the controlling scheme has enhanced under stator coil resistance variation, the dynamic behavior of the BLDC motor under load torque variation is not sufficiently improved while many computational efforts have been burdened.

Recently, machine learning-based controlling algorithms for motor driver has been extensively used in several applications [31]. A new convolutional neural network (CNN) based controlling scheme for a BLDC motor is proposed in [32]. In this method, CNN has been used to optimize the parameters of the integral square error of the PID controller in actual implementation. Mission profile data based on the mathematical model of the BLDC motor is collected for training and testing processes. However, the proposed method is not robust during external load torque disturbance and motor parameters' uncertainties. Busetto et al. [33] propose a new data-driven neural network algorithm for field-oriented control (FOC) of BLDC motor. In this algorithm, the tuning of the FOC parameters are formulated as a model reference optimization problem which makes this algorithm a potential candidate for the set membership global optimization of FOC. In comparison with Bayesian optimization, although this proposed method is less computationally expensive, converging of this optimization may last longer, causing problems in applications with the high number of design constraints.

In the papers mentioned above, the attention has been mainly concentrated on applying modern tools, such as neural networks, and data-driven machine learning to optimize the controlling parameters in different controlling algorithms, including sliding mode, fuzzy logic and conventional controllers. The researchers rarely focus on the direct use of

a deep neural network (DNN) in BLDC motor controlling based on traditional methods. This paper presents a direct benefit of DNN in controlling an SP BLDC motor. In addition, we put another step forward and try to simultaneously take advantage of two conventional controlling algorithms, namely PID and linear–quadratic regulator (LQR), by utilizing them in characterizing two distinct DNNs. Simultaneous exploitation of this combination improves the global performance of the controlling system. In this regard, we employ the mixture of experts (MoE) algorithm to use both merits of LQR and PID controllers. A gating network, as the core of MoE, is trained to determine the contribution of each controller on the final stage of the controlling index, namely the modulation index.

The organization of this paper is as follows: modeling and finite element analysis of the single-phase permanent magnet BLDC external rotor motor are explained in section II. While section III deals with implementing controlling strategies, the results and discussion are expressed in section IV, and a conclusion is drawn in the final section.

## II. MODELING OF SP PMBLDC ER MOTOR

In this section, a dynamic model of the BLDC motor of interest is established based on FEA and a dynamic model for the SP PM BLDC ER motor.

### A. 2-D FINITE ELEMENT ANALYSIS

The permanent magnet material has a direct effect on the power density of the SP PM BLDC ER motor. In other words, the higher the flux density the permanent magnet has, the higher power can be achieved in a fixed permanent magnet volume. Thus the SP PM BLDC ER motor considered here uses an Nd-Fe-B magnet ring placed on the rotor as shown in Fig. 1.

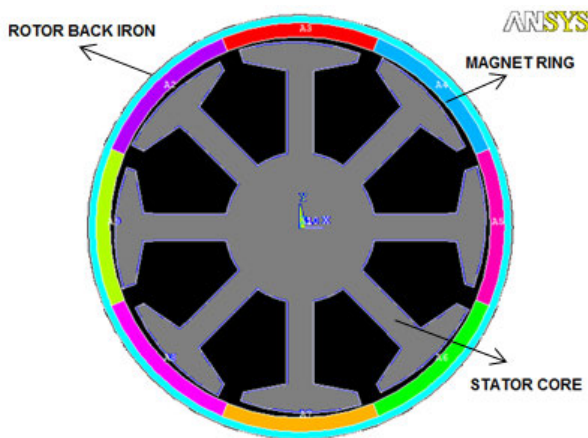


FIGURE 1. A sectional view of SP PM BLDC ER motor without windings.

The stator poles are asymmetrically designed to provide the ability of self-starting in the single-phase BLDC motor. These non-uniform air gaps, although they easily support the self-starting of the motor, some undesirable torque ripples

TABLE 1. Parameters and dimensions used in the finite element analysis.

Parameters and Dimensions	Values
Maximum source voltage (V)	190
Output power (W)	80
Number of pair poles	4
Rated speed (rpm)	360
Stator resistance (ohm)	8
Stator inductance (H)	0.042
Rotor inertia (Kg.m <sup>2</sup> )	0.0008
Outer diameter (mm)	90
Average radial air gap length (mm)	1
Stator core length (mm)	10
PM radial thickness (mm)- Nd-Fe-B	3
Number of coil turns	1000
PID controlling coefficients	K <sub>p</sub> =2.089, K <sub>i</sub> =9.3456, K <sub>d</sub> =0.013
LQR controlling coefficients	K=[45.344 53741 0] K <sub>r</sub> =100

called cogging torque are induced on the out of the shaft of the motor, which has to be considered in our controlling design procedure. The stator laminations and rotor back iron are made of steel and soft iron, respectively. The SP PM BLDC ER motor is an eight-pole machine with only one coil per stator pole. The parameters and dimensions are given in Table 1.

The model had 25366 elements and 38982 nodes. The mesh size optimization is performed using a mesh operation tool in Maxwell software in which one may also be able to define some constraints and conditions to optimize the accuracy of the simulation. In the pole edges and magnetic bars, the maximum mesh length is limited to 1mm. Based on these constraints, the software proposes the best mesh sizes through the different parts of the model. The stator coils are externally supplied through the excitation management tool of the Maxwell software regarding a predefined single-phase full bridge inverter. Finite element analysis (FEA) was used to obtain the electromotive force (EMF) induced in the coils and the created cogging torque on the motor shaft for better SP PM BLDC ER motor modeling. In this type of motor, EMF constant (K<sub>e</sub>) varies with rotor angular displacement. It is owing to a non-uniform air gap [34], [35]. The EMF constant could be obtained from the calculation of flux linkage passing through the coils via the stator core using the following expression [36]:

$$K_e = \frac{\Delta\lambda}{\Delta\theta_r} \tag{1}$$

where  $\lambda$  is the flux linkage of coils connected in series and  $\theta$  is the rotor position. Thus with evaluating the  $\Delta\lambda$  to  $\Delta\theta_r$  ratio, calculation of K<sub>e</sub> will be possible. It becomes easy using 2D FEA, as shown in Fig. 2. It illustrates the paths of magnetic flux via stator core without any external excitation. By using the above procedure, EMF constant will be estimated. Fig. 3a demonstrates the EMF constant evaluated by FEA and its fundamentals harmonic with the following expression (the EMF

constant is in terms of the stator pair poles) [34], [36]:

$$K_e^{fundamental} = 4.8 \cdot \sin(4 \cdot \theta_r) \text{ vs/Rad} \quad (2)$$

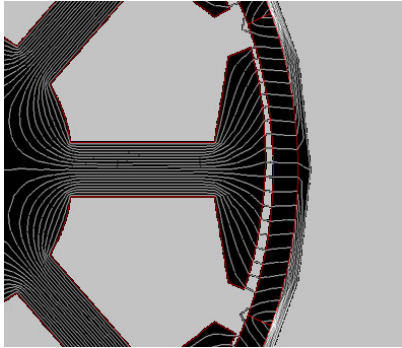


**FIGURE 2.** Flux linkage through per coil using 2D finite element analysis in ANSYS/Maxwell environment. The magnetic and physical parameters of the simulation are listed in Table 1.

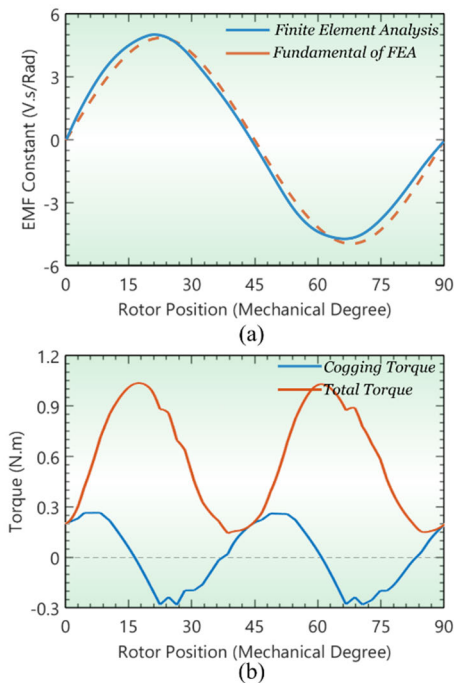


**FIGURE 3.** Exploitation of mechanical and electrical parameters for SP BLDC ER motor of interest. a) Flux linkage variations and b) total torque variations extracted from FEA, in every rotor position a non-zero starting torque would be produced owing to the cogging torque existence.

Regarding aforementioned equation and Fig. 3a, one can obtain that a cycle of the electromotive force (EMF) induced in any of the stator coils is completed during 90° mechanical rotor revolution. In other word, in each mechanical rotor revolution, four electrical cycles are completed. This relation, as written (2), can be expounded by the use of pair poles definition in the motor as  $\theta_{elec} = \theta_r \cdot P/2$  in which  $\theta_r$  and  $\theta_{elec}$  represent the mechanical and electrical angles in term of degree and  $P/2$  denotes the pair poles of the motor.

The effective value of EMF constant is calculated as follows:

$$K_e^{effective} = 3.394 \text{ vs/Rad} \quad (3)$$

For calculating cogging torque in the SP PM BLDC ER motor, storing energy should be evaluated while there is not any external excitation. Cogging torque is expressed by the following equation [36]:

$$T_{cogging} = \frac{\Delta w_f}{\Delta \theta_r} \quad (4)$$

It is directly obtained from finite element software by evaluating the energy storage variation to the rotor angular variation ratio. Fig. 3b demonstrates the total and cogging torques, which may be written as (the cogging torque is in terms of the stator poles) [34], [36]:

$$T_{cogging}^{fundamental} = -0.2678 \cdot \cos(8\theta_r + 22.1^\circ) \quad (5)$$

The interaction between the magnetic field of the stator coils and the permanent magnets of the rotor produces electromagnetic torque ( $T_e$ ). Total torque is the sum of the electromagnetic torque and the cogging torque ( $T_{cogging}$ ). As shown in Fig. 3b, the total torque in every rotor position has non-zero value which is leading to self-starting of the SP PM BLDC ER motor owing to existence of asymmetric air gap.

### B. DYNAMIC MODEL OF SP PM BLDC ER MOTOR

The global model of the SP PM BLDC ER is shown in Fig. 4. This model has different parts required to be modeled [34], [37]. Mechanical and electrical modeling of this motor, including voltage and torque equation models are discussed in this section. The motor model is based on the well-known voltage and torque equations of the DC motor. Thus the voltage equation is [36]:

$$v_a = e_a + R_a i_a + L_a \frac{di_a}{dt} \quad (6)$$

where  $v_a$  is the inverter voltage,  $R_a$  and  $L_a$  are stator resistance and stator inductance, respectively.  $e_a$  is the back EMF of the motor and is defined as the following expression [36]:

$$e_a = K_e(\theta_r) \cdot \omega_r \quad (7)$$

where  $K_e$  is the EMF constant, which is a function of rotor position and  $\omega_r$  is the motor speed. Fig. 4 illustrates the voltage equation model.  $v_a$  is the output voltage of the inverter and its polarity is a function of rotor position. Based on the torque balance principle representing that sum of the loading torques equals to sum of the producing torques [36], the torque equation of this machine is calculated as:

$$T_e + T_{cogging} = J \frac{d\omega_r}{dt} + B_m \omega_r + T_L \quad (8)$$

where  $J$  is the inertia of rotor and load coupled,  $B_m$  is friction constant,  $T_L$  is torque needed by load,  $T_{cogging}$  is cogging torque obtained from FEA and  $T_e$  is electromagnetic torque which is expressed by the following equation [38]:

$$T_e = K_e(\theta_r) \cdot i_a \quad (9)$$

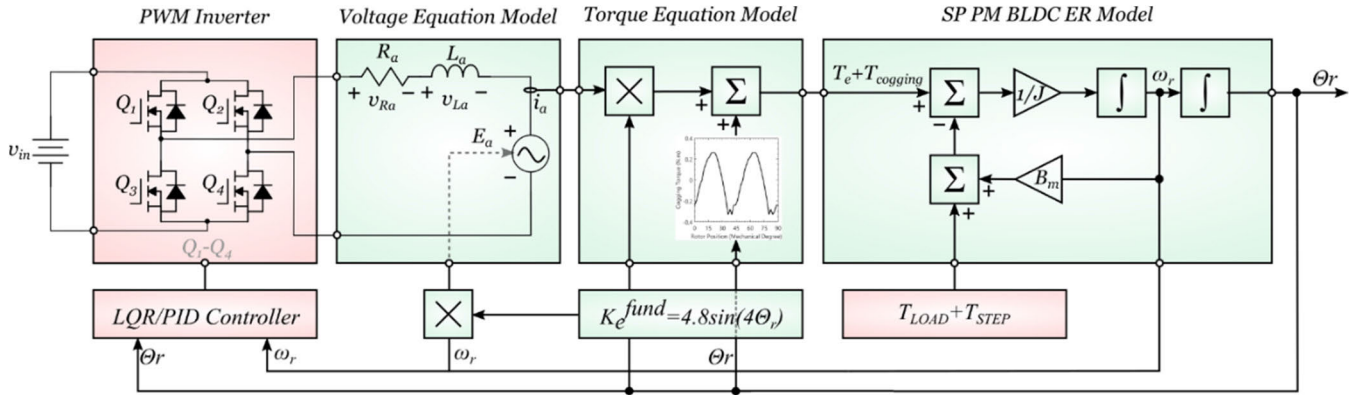


FIGURE 4. Global modeling of the single-phase permanent magnet BLDC external rotor motor.

A full-bridge single-phase PWM inverter has been utilized to supply the SP PM BLDC ER motor. The inverter is demonstrated in Fig. 4 (red-shaded). Motor speed is controlled by changing the modulation index ( $m_a$ ) of the PWM inverter. The gates are driven based on rotor position feedback. In this paper, although carrier voltage amplitude ( $V_c$ ) is constant, reference voltage amplitude ( $V_{ref}$ ) could be varied concerning motor speed, which leads to a change in inverter output voltage. More details can be found in [39]. This motor's torque should take over at least minimum load torque which has a step increase in operating time, load and rotor inertia, and friction torque. The load model has shown in Fig. 4 in the last part.

### III. CONTROL OF SINGLE PHASE PERMANENT MAGNET BRUSHLESS DC MOTOR

Using closed-loop control makes substantial quantities be in the desired values. Although closed-loop control increases the cost of products, it could increase efficiency and guarantee the desirable values or set points. Finding a cost-effect and fast response controlling method for special motors has sparked off a heated debate in recent years. In this section, two methods are proposed, and their advantages and drawbacks have been discussed. Then, the MoE algorithm is proposed to combine both controllers' specifications.

#### A. CONTROLLING PRINCIPLE AND DESIGN

In this section, the principles of the two following controlling strategies will be discussed.

One of the most common closed-loop controllers is the PID controller) which is tremendously adopted in industrial control systems. The error of a measured value and a reference value is the driving force of a PID controller. By using this controller, an error can be minimized by adjusting the control inputs. Fig. 5 illustrates the standard structure of the PID controller. In this structure, the control variable  $u(t)$  is defined by summing three diverse terms affected by the tracking error  $e(t)$ .  $K_p$  determines that this term is proportional to the error.  $K_i/S$  denotes an integral term, and  $K_dS$

is a derivative term. Each of terms mentioned above works separately [40], [41], [42].

The theory of optimal control deals with operating a dynamic system at minimum cost. The dynamics of the system are defined by state variables, and the cost function is determined by a quadratic function called the LQ problem. The linear-quadratic regulator (LQR) is our tool to minimize the cost function [43]. The system state equations can be written in the following form [44]:

$$\begin{aligned} \dot{x} &= Ax + Bu \\ y &= Cx + Du \end{aligned} \tag{10}$$

Using state feedback

$$u = -Kx \tag{11}$$

Using LQR for minimizing J to minimize the cost [43]

$$J = \int_0^{\infty} x^T Qx + u^T R u dt \tag{12}$$

where J is the cost function and should be minimized. Q and R are state and input weighting arrays, respectively. These matrices are generally obtained by trial and error. K is obtained from the following expression.

$$K = R^{-1} B^T P \tag{13}$$

P is obtained from the following Ricatti equation [45]

$$A^T P + PA - PBR^{-1} B^T P + Q = 0 \tag{14}$$

Fig. 5b depicts the control block diagram of the control system. As observed, an integrator is used to have zero steady-state error. Obtaining system state equations or transfer function is always necessary to design a control algorithm. Block diagrams, which demonstrate the interconnection of the system equations, are widely employed in control system investigation and design.

The voltage equation and the relationship between torque and rotor speed of the SP PM BLDC ER motor may be written as (5)-(8).

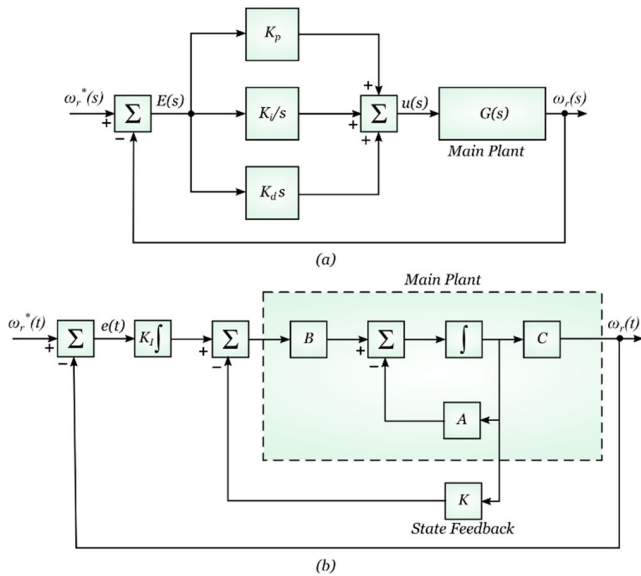


**FIGURE 5.** Controlling schematics for single phase permanent magnet BLDC external rotor motor. a) Conventional PID, b) LQR.

Here, these equations must be written in terms of state variables which are armature current, rotor speed, and rotor position, respectively.

$$\frac{di_a}{dt} = \frac{1}{L_a}(-R_a i_a - K_e \omega_r + V_a) \quad (15)$$

$$\frac{d\omega_r}{dt} = \frac{1}{J}(K_e i_a - B_m \omega_r - T_L + T_{cogging}) \quad (16)$$

$$\frac{d\theta_r}{dt} = \omega_r \quad (17)$$

where  $T_{cogging}$  and  $K_e$  are nonlinear functions of  $\theta_r$ . That means by applying for Taylor extension over their equilibriums via using their fundamentals (2) and (5), one can reach out the dynamic behavior of the system.

PID controlling technique is a controlling system based on the error between the reference and measured output value. Using this error to reach a reference output value by adjusting the input value which here is the input voltage  $V_a$ . PID coefficients may be selected so that the needed rise time, Overshoot, settling time, and steady-state error of the system are satisfied. Therefore, catering to our purposes, the following coefficients are calculated using MATLAB tools

$$K_p = 2.089, \quad K_i = 9.3456, \quad K_d = 0.013 \quad (18)$$

LQR controlling technique is a type of controlling system based on state feedback. The algorithm of gaining state feedback matrix  $K$  is thoroughly described in the previous section. Concerning matrix  $A$ , which is easily borne out from (15)-(17) and mentioned linearization method,  $K$  is

$$K = [45.344 \quad 53741 \quad 0] \quad (19)$$

$K_i$  is also selected regarding the bandwidth of the controlling system, and here by trial and error via simulations are chosen 100.

### B. DEEP NEURAL NETWORKS AND MIXTURE OF EXPERTS APPLICATION

The behavior of the SP BLDC ER motor of interest can be controlled through adjusting its input voltage. Accordingly, by tuning a modulation index of the inverter, one can easily tune the speed of the SP BLDC ER motor. As previously mentioned, we use two different types of controlling systems i.e., PID and LQR. In both controllers, the aim is to adjust  $m_a$  in such a way as to minimize the error between the measured and the reference speed. Two distinct deep neural networks (DNNs) are constructed and trained for each LQR and PID based on several operating points (2850 different operating conditions are considered in this study). The first two networks in Fig. 6 depict the proposed neural network structures. Each DNN has four internal layers with a number of neurons of [15 15 20 15]. The number of neurons and hidden layers of each DNN have been selected as a trade-off between the accuracy of the DNN and the required time of the training process via trial and error.

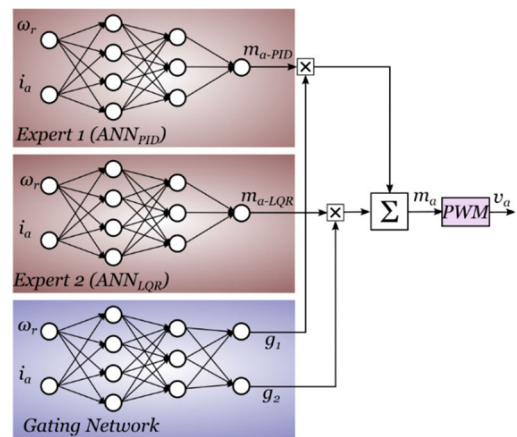


**FIGURE 6.** Architecture of a mixture of experts (MoE) consisting of two expert networks and a gating network. Given an input  $x \sim (\omega_r, i_a)$ , the output  $y \sim m_a$  of the system is computed as the sum  $m_a = m_{a-PID} \cdot g_1 + m_{a-LQR} \cdot g_2$ .

As an example, Fig. 7 demonstrates the correlation between the training process time and model accuracy regarding the number of hidden layers and their corresponding number of neurons in PID-DNN. As observed, several tests have been performed to obtain the best structure of PID-DNN via selecting different numbers of hidden layers and neurons. Although the accuracy of the model increases by increasing the number of layers and neurons, the computational time for the training process significantly enlarges. In the low number of hidden layers and neurons, the PID-DNN training process time becomes considerably lower. However, its accuracy does not meet the requirements of our problem. The green circles specify the optimum number of neurons for each number of hidden layers. One can find that the minimum RMSE and computational time are allocated to a four-hidden layer structure with a number of neurons between 15 and 20 for each hidden layer.

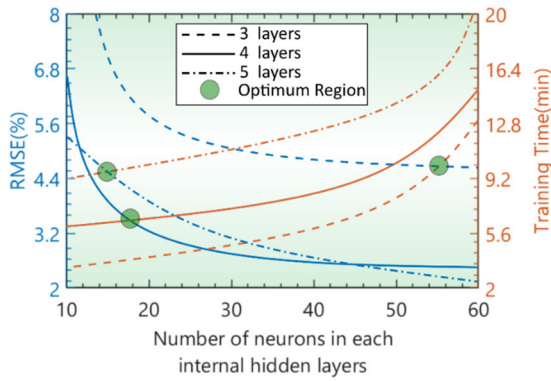


**FIGURE 7.** A trade-off between training process time and accuracy of PID-DNN as the functions of the number of hidden layers and the number of neurons.

Using these 2850 datasets, the DNNs are trained in such a way as to minimize the root mean square error (RMSE) of the predicted  $m_a$  and the actual  $m_a$  as follows [46]:

$$RMSE = \sqrt{\sum_{i=1}^n \frac{1}{n} (\hat{m}_{a-i} - m_{a-i})^2} \quad (20)$$

where  $\hat{m}_{a-i}$  and  $m_{a-i}$  are predicted and actual modulation index, respectively. Back-propagation and k-fold methods are used for the training and validating processes.

The gating network, as the core of MoE, is in charge of determining the contributions of each expert i.e.,  $m_{a-PID}$  and  $m_{a-LQR}$ , on the final modulation index i.e.  $m_a$ . Similar to DNNs, the same optimization process is applied to the gating network characterize the optimum structure of the network. The gating network has four hidden layers with a structure of [25 30 25 30]. It means that the minimum RMSE and computational time occur while the construction has four hidden layers with the abovementioned number of neurons. MoE tries to obtain a set of weighting factors for each neuron of the gating network to minimize the RMSE. The unity constraint ( $g_1 + g_2 = 1$ ) of the gating signal is vital in the training process of the gating network. Using maximum likelihood, one can determine the weighting factors of the gating network by maximizing the following equation [47]:

$$L(\theta) = \prod_{\alpha} P(x^{\alpha}, y^{\alpha} | \theta) = \sum_{\alpha} \log \sum_j g_j(x^{\alpha}, V) N_j e^{-\frac{1}{2\sigma_j^2} (y^{\alpha} - f(x^{\alpha}, W_j))^2} \quad (21)$$

where  $x$  is the input vector, and  $W$  is the weighting factor of the gating network. By solving the constraint mentioned earlier, the MoE (gating network) is trained. The combination of the PID and LQR controllers will lead to a more reliable and robust controlling strategy as will be discussed in the next section.

#### IV. RESULTS AND DISCUSSION

In machine learning-based strategies, measurement of the DNNs' training process accuracy is of paramount. Several

indices, such as root mean square error, maximum absolute error, and coefficient of determination are potential candidates for evaluating the accuracy of the DNNs. In this paper, RMSE has been chosen to investigate how PID and LQR DNNs implement. Fig. 8 demonstrates the predicted and actual  $m_a$  for both controllers' DNNs, namely LQR-DNN and PID-DNN. As shown, the results are linearly correlated with each other at the vicinity of the perfect prediction (dashed line). The RMSEs are 3.4% and 4.1% for PID and LQR deep neural networks. The data for LQR-DNN is a bit more dispersive in comparison with PID-DNN. It originates from the fact that in the LQR controller, the state variables directly affect the modulation index. Regarding this figure, one can validate the performance of the DNNs in both PID and LQR strategies.

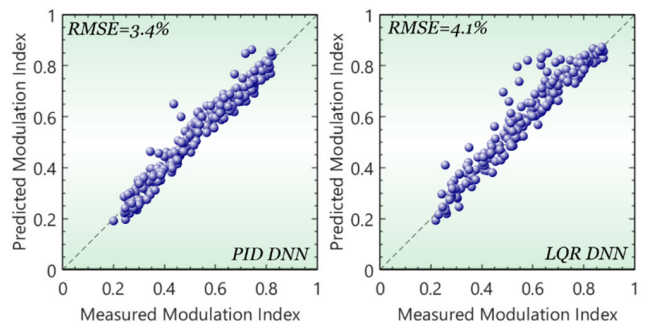


**FIGURE 8.** Performance of the deep neural network using PID and LQR controller for the SPBLDC ER motor of interest.

Fig. 9 illustrates the normalized status of the considered state variables (input), namely  $i_a$  and  $\omega_r$ , for all three controlling strategies for 200 operating points. In this figure, the dispersion of operation points are demonstrated in the similar rotor speed operating points for all three controlling strategies, namely PID, LQR and MoE. In the PID controller, the variation of armature current is 60.3%. This variation is about 72.1% for LQR controlling strategy. It shows that the driving circuit requires to supply more severe armature current fluctuations for SP PM BLDC ER motor than that of in PID controller in the identical operating points. This wider armature current variation (11.8%) can impose more power loss in the inverter and also increase the over/undershoot of the rotor speed. However, regarding Fig. 9c, one can obtain that the required armature current variation is limited to 54% in the MoE controlling strategy. Accordingly, the merits of lower armature current variation in the optimized combination use of PID and LQR i.e. MoE strategy can improve the dynamic behavior of the controller compared to the PID and LQR controllers.

The objective of this paper is to apply MoE controlling strategy to an SP PM BLDC ER motor and guarantee its improved performance either in steady state or transient conditions. In this regard, in addition to MoE implementation, five other controlling strategies, including sliding mode (SM), fuzzy neural network (FNN), convolutional neural network (CNN), conventional PID, and conventional LQR,

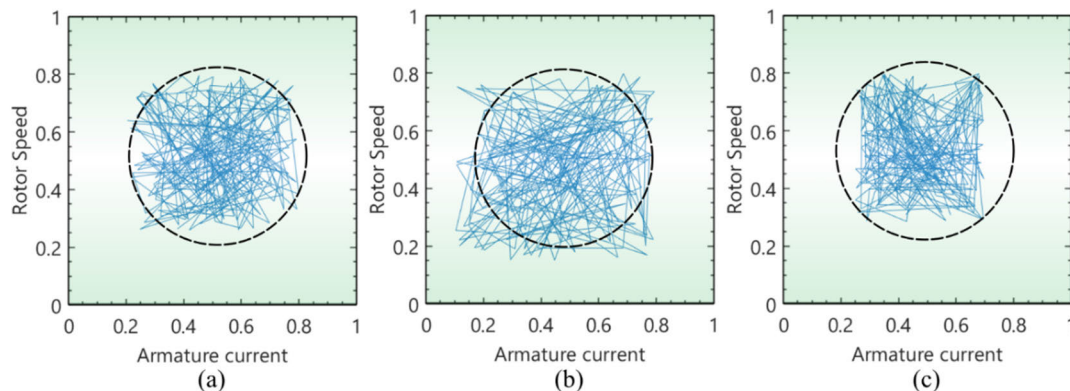


**FIGURE 9.** Distribution of the state variable for 200 different operating points in a) PID-DNN, b) LQR-DNN, and c) MoE controlling strategies, for SP BLDC ER motor. It reveals that in the MoE strategies the dynamic behavior of the SP BLDC ER motor is improved owing to the application of both merits of PID and LQR controller.

are taken into account to provide a fair comparison. More details of FNN, CNN, and SM controlling strategies can be found in [26], [29], and [48]. The dynamic behavior of the SP PM BLDC ER motor over a step-change in the load torque from half of the rated torque to its rated (0.5 N.m to 1 N.m) and its performances over a step-change in its speed reference from 360 rpm to 300 rpm are simulated and shown in Fig. 10 and Fig. 11, respectively. In each analysis, the procedure of the controlling strategies will be compared.

Dynamic responses (rotor speed and armature current) of the SP PM BLDC ER motor of interest under a step change in load torque is depicted in Fig. 10 for MoE, SM, FNN, and CNN controlling strategies. Fig. 10a illustrates the mechanical response using the MoE, sliding mode (SM), fuzzy neural network (FNN) and convolutional neural network (CNN) controllers. The rotor speed experiences a decrease during applying rating torque from its initial value, namely half-rated. The mechanical response at the torque release demonstrates an overshoot in rotor speed.

This is the case for all four strategies. However, the performance of rotor speed controlling can be judged via two well-known parameters i.e., under/overshoot and settling time. Among all demonstrated strategies, FNN has the best performance in terms of the settling time, which is about 8 ms. The MoE, SM, and CNN have settling times of 9.2 ms, 16 ms, and 16ms, respectively. The settling time for LQR and PID (their waveforms are not shown owing to keeping the figure as direct as possible) is 8 ms and 15.3 ms, respectively. Based on the maximum settling time, one can find that LQR and FNN have the best response among all strategies. They are followed by the MoE algorithm with an insignificant increase. The fast dynamic response of LQR originates from the fact that the controller directly uses the state variables leading to a speedier reaction to any kind of variation. The acceptable response of the FNN algorithm is due to its self-training process in which increases the share of the critical input parameter by tuning the rules. The delay in the PID strategy originates due to the integral coefficient in the controller, which lags the controlling variable leading

to a slower dynamic response. Another contributory factor in comparing the dynamic behavior of strategies as mentioned earlier is undoubtedly the overshoot/undershoot of the rotor speed. As shown in Fig. 10a, one can obtain that the best overshoot/undershoot is dedicated to MoE controlling strategy with a maximum value of 1.8%. SM, FNN, and CNN have 2.26%, 2.9%, and 2.5%, respectively. In the meanwhile, all the modern strategies are better than that of using conventional LQR strategy in which it suffers from 3% overshoot/undershoot during load torque variation. On the other hand, the traditional controller has better conditions than all strategies by having only 1.1% overshoot/undershoot. With this information, one can attain that MoE controlling method is the combination of LQR and PID controllers and harvesting their advantages while mitigating each other detriment. The electrical dynamic response of the considered algorithms is demonstrated in Fig. 10b. Regarding this figure, it is observed that CNN and SM have the worst transient behavior during each switching period. In this case, FNN and MoE strategies have the best conditions. In addition, MoE experiences a lower current ripple in the steady state condition, which will lead to a lower torque ripple on the motor shaft. It also leads to lower switching loss, and higher efficiency in the inverter.

The dynamic behavior of the considered SP PM BLDC ER motor under reference speed variation is shown in Fig. 11. The rotor speed is shown in Fig. 11a for MoE, SM, FNN and CNN controlling strategies. The results validate our observations in the previous load torque step changes. From the settling time point of view, FNN and MoE have the shortest settling time among the modern controllers (They are 8 ms and 9 ms, respectively). The maximum settling time (15 ms) belongs to the SM method regarding Fig. 11a. However, among all controlling strategies, including modern, and conventional ones, LQR has the best performance with 7ms settling time, and PID has the worst performance with 15.1 ms. Rotor speed undershoot/overshoot follows the previous pattern and PID has the lowest one with 2%, while the highest is dedicated to LQR with 5.9%. MoE, SM, CNN, and FNN serve 2.1%, 4.2%, 4.7%, and 5.8%, respectively. Based



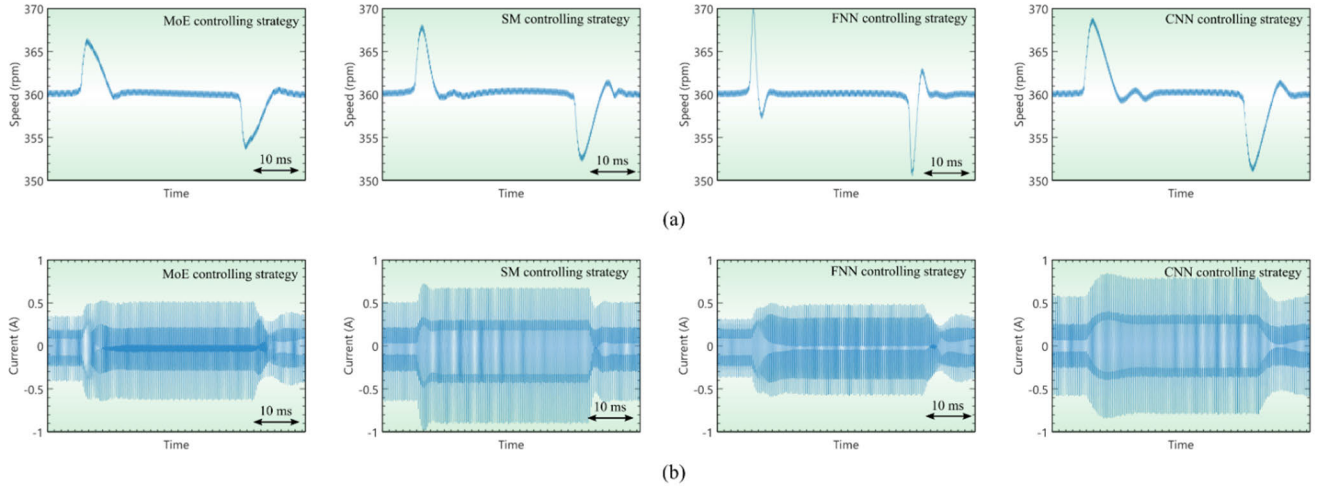


**FIGURE 10.** Dynamic response of SP PM BLDC ER motor (rotor speed and armature current) under load torque step change using MoE, SM, FNN and CNN controllers. a) Rotor speed variation, b) armature current.

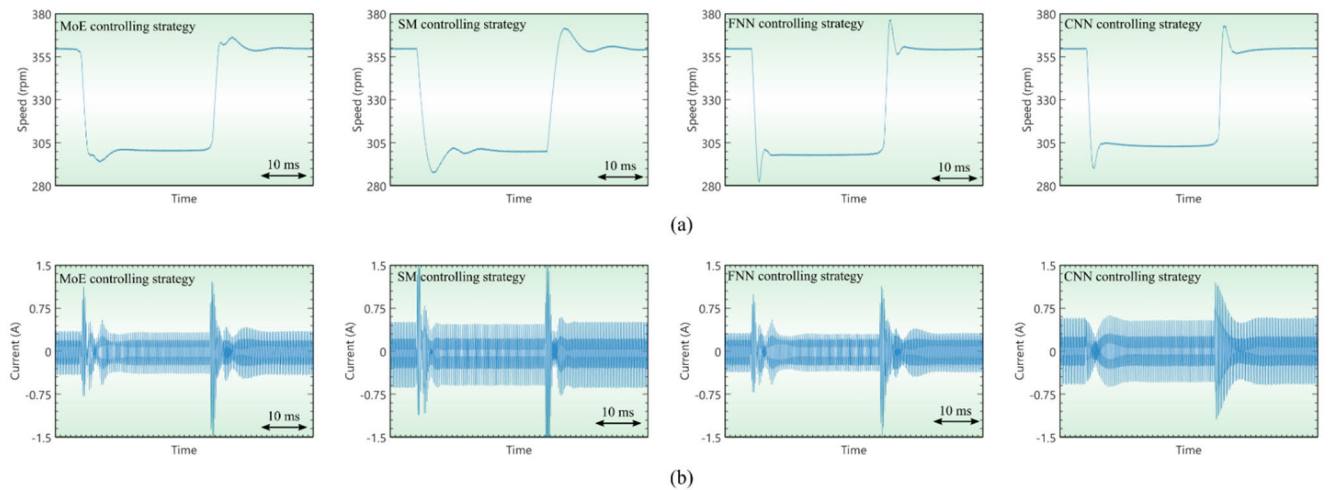


**FIGURE 11.** Dynamic response of SP PM BLDC ER motor (rotor speed and armature current) under reference speed step change using MoE, SM, FNN and CNN controllers. a) Rotor speed variation, b) armature current.

**TABLE 2.** Feature extraction of different controlling strategies.

Control strategy	Maximum Under/overshoot (%)		Maximum Settling time (ms)		Torque ripple (%)		Maximum Switching Freq. (kHz)	
	Sim.	Exp.	Sim.	Exp.	Sim.	Exp.	Sim.	Exp.
	MoE	2.1	2.7	9.2	11.3	18.3	23.2	12.1
PID	2.0	2.3	15.3	16.5	16.4	22.6	12.0	12.0
LQR	5.9	6.3	8.0	9.1	30.1	38.3	20.4	20.9
CNN	4.7	5.2	16.0	16.5	23.2	26.8	16.7	17.1
FNN	5.8	6.3	8.0	8.2	18.0	22.4	14.9	16.2
SM	4.2	4.8	16.0	16.9	28.6	33.7	24.3	25.3

on the disclosed results under speed reference changes, one can observe that the proposed MoE algorithm has the best performance in regard to settling time and overshoot/undershoot considerations. It is since MoE has taken advantage of both PID and LQR controllers. The electrical dynamic behavior of the considered SP PM BLDC ER motor is drawn in Fig. 11b. In this case, the armature current waveforms validated those observations in the previous load torque variation.

A qualitative comparison between the proposed MoE controlling strategy and other conventional and modern controllers is illustrated in Fig. 12. In this figure, four critical factors in evaluating the performance of any kind of controlling strategy are discussed. From the undershoot/overshoot point of view, only a conventional PID controller has a better condition than the proposed method at the expense of losing fast dynamic tracking. Other strategies have worse performance, while LQR is the worst one. This ranking is held in both load torque disturbance and speed reference variation as denoted with different colors in the most left figure. Regarding the settling time, the LQR controller has the best condition, and MoE lays in the second rank. The MoE is trained in such a way as to benefit from the advantages of both LQR and PID since they are a good complement to each other. This fact is held in both load torque disturbance and speed reference variation. The proposed method also has an acceptable behavior in steady state operation.

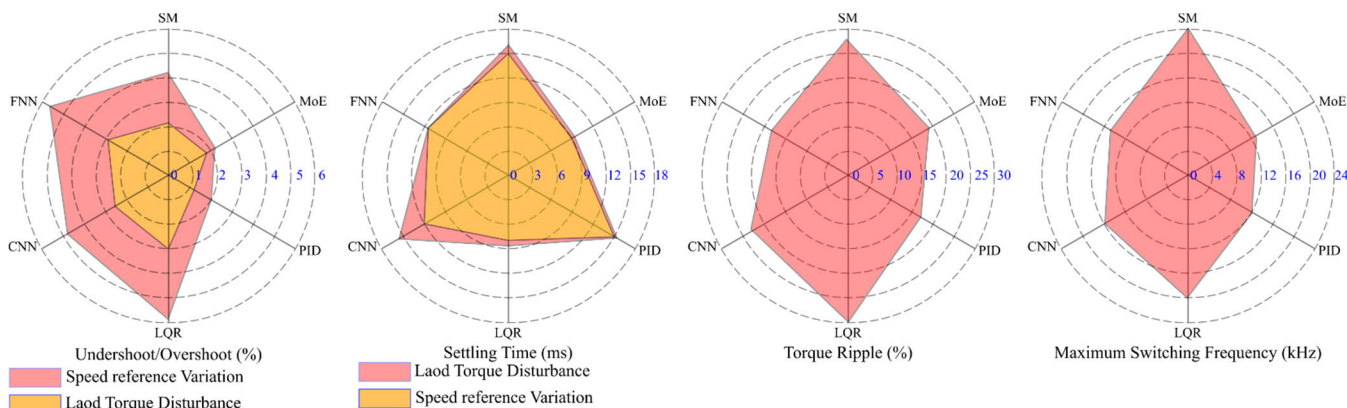


**FIGURE 12.** Investigation of four critical factors, including undershoot/overshoot, settling time, steady state torque ripple, and maximum switching frequency on the final performance of BLDC motor controller using MoE, SM, FNN, CNN, LQR, and PID.

The experimental results for these features are listed in Table 2 under applying all six modern and conventional controlling methods. On the whole, the experimental results validate the simulation results under using different controlling strategies. The experimental results also reveal that MoE controlling method can be an appropriate strategy in which both steady state and dynamic behaviors are optimized in comparison with other strategies.

Regarding Fig. 12 and Table 2, one can observe that the torque (current) ripple of the considered BLDC motor experiences its minimum value in the MoE strategy. This phenomena occurs since the gating network is well-trained and assumes a significant contribution to the PID-DNN in the steady state to minimize the switching frequency and torque ripple. The gating network increases the contribution of LQR-DNN in transient conditions in which faster response is required.

To explore the operation of the proposed algorithm for a BLDC motor, an experimental setup was implemented. An SP BLDC ER motor with the specifications listed in Table 1 was employed. The controller algorithm was performed through an STM32F407VGT6 discovery board. The trained parameters (weighting factors) of LQR-DNN, PID-DNN, and gating network were all inserted into the microcontroller via defining several arrays. The armature current and the rotor speed were sensed via a Hall Effect sensor and an encoder. The analog measured data was then converted to digital using two ADC modules of the microcontroller. Based on the rotor speed and armature current, the MoE generates a switching signal which transfers to a switching pattern based on a predefined look-up table. The experimental results of rotor speed and the electromagnetic torque under a sudden step change and gradual sinusoidal speed reference are depicted in Fig. 13. In the first case in which the speed reference experienced a sudden change (from 210rpm to 260 rpm and vice versa), the MoE controlling strategy was tracking the reference speed well. The maximum overshoot/undershoot is limited to 2.8%. The settling time is limited to maximum of 12 ms. The electromagnetic torque ( $T_e$ ) has an acceptable ripple value. The performance of the considered BLDC motor

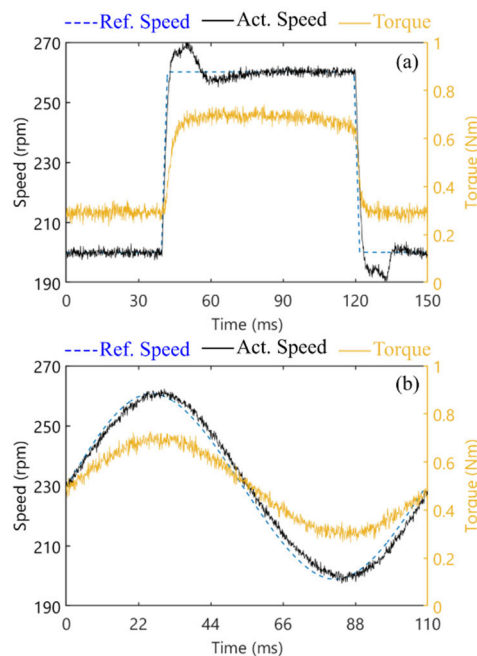


**FIGURE 13.** Experimental results of the considered BLDC in the conditions of a) sudden step change and b) gradual sinusoidal change of the speed reference.

has got even better with gradual speed reference change. As shown in Fig. 13b, the actual speed tracked the reference speed with a minimum delay value, namely less than 1ms. Regarding these figures, one can find that the experimental results validate the merits of the new proposed algorithm (MoE strategy) thanks to the intelligent combination of two conventional techniques (PID and LQR).

The detriment of this controlling scheme is the fact that the designer requires to design several controllers based on the number of employed experts in the MoE. This may burden some extra time in the designing stage. It even gets worse by increasing the number of experts in the proposed MoE. However, some optimization approaches may be apply to minimize the designing stage time by optimizing the number of training data.

## V. CONCLUSION

A new mixture of experts-based controlling strategy is presented in this paper. A 2D static FE analysis was performed and the quantities (cogging torque, and EMF constant) were extracted and used to implement a dynamic motor model. The exploited dynamic model was used in designing different controlling algorithms, namely PID, LQR, and MoE strategies using deep neural networks. The MoE strategy tried to find an optimum contribution factor of PID and LQR using a trained gating network. The results reveal significant improvement in dynamic and steady-state behavior of the SP BLDC ER motor of interest while performing MoE-based controlling strategy. The steady-state ripple became lower in this theme, leading to lower power loss and higher efficiency. We are now focusing on optimizing the number of data for the training process to minimize the designing time, and the results will be presented in the near future.

## REFERENCES

- [1] A. Attar, J. Bouchnaif, and K. Grari, "Control of brushless DC motors using sensorless back-EMF integration method," *Mater. Today*, vol. 45, pp. 7438–7443, Jan. 2021, doi: [10.1016/j.matpr.2021.01.861](https://doi.org/10.1016/j.matpr.2021.01.861).
- [2] M. K. Umam, R. N. Hasanah, and T. Nurwati, "PID-based fuzzy logic theory implementation on BLDC motor speed control," in *Proc. Int. Seminar Intell. Technol. Appl. (ISITIA)*, 2022, pp. 407–412, doi: [10.1109/ISITIA56226.2022.9855291](https://doi.org/10.1109/ISITIA56226.2022.9855291).
- [3] H. Wang, J. Wang, X. Wang, S. Lu, C. Hu, and W. Cao, "Detection and evaluation of the interturn short circuit fault in a BLDC-based hub motor," *IEEE Trans. Ind. Electron.*, vol. 70, no. 3, pp. 3055–3068, Mar. 2023, doi: [10.1109/TIE.2022.3167167](https://doi.org/10.1109/TIE.2022.3167167).
- [4] H. Jin, G. Liu, and S. Zheng, "Commutation error closed-loop correction method for sensorless BLDC motor using hardware-based floating phase back-EMF integration," *IEEE Trans. Ind. Informat.*, vol. 18, no. 6, pp. 3978–3986, Jun. 2022, doi: [10.1109/TII.2021.3113368](https://doi.org/10.1109/TII.2021.3113368).
- [5] W. Lee, D. Han, and B. Sarlioglu, "Comparative performance analysis of reference voltage-controlled pulse width modulation for high-speed single-phase brushless DC motor drive," *IEEE Trans. Power Electron.*, vol. 33, no. 5, pp. 4560–4568, May 2018, doi: [10.1109/TPEL.2017.2731962](https://doi.org/10.1109/TPEL.2017.2731962).
- [6] A. S. Al-Adsani, M. E. AlSharidah, and O. Beik, "BLDC motor drives: A single Hall sensor method and a 160° commutation strategy," *IEEE Trans. Energy Convers.*, vol. 36, no. 3, pp. 2025–2035, Sep. 2021, doi: [10.1109/TEC.2020.3046183](https://doi.org/10.1109/TEC.2020.3046183).
- [7] P. Mishra, A. Banerjee, and M. Ghosh, "FPGA-based real-time implementation of quadrature-duty digital-PWM-controlled permanent magnet BLDC drive," *IEEE/ASME Trans. Mechatronics*, vol. 25, no. 3, pp. 1456–1467, Jun. 2020, doi: [10.1109/TMECH.2020.2977859](https://doi.org/10.1109/TMECH.2020.2977859).
- [8] H. Hwang, J. Cho, S.-H. Hwang, J. Choi, and C. Lee, "Design of a single-phase BLDC motor for a cordless vacuum cleaner considering the efficiency of airflow," *Energies*, vol. 12, no. 3, p. 465, Feb. 2019, doi: [10.3390/en12030465](https://doi.org/10.3390/en12030465).
- [9] S. Sashidhar and B. G. Fernandes, "Comparison of a ferrite based single, three-phase spoke and surface permanent magnet BLDC motor for a PV submersible water pump," in *Proc. IEEE Int. Conf. Ind. Technol. (ICIT)*, Mar. 2015, pp. 671–676, doi: [10.1109/ICIT.2015.7125175](https://doi.org/10.1109/ICIT.2015.7125175).
- [10] M. Zhao, X. Ran, and J. Shang, "Influences of 3D fluid field for submersible permanent magnet motors on thermal field distribution," in *Proc. 22nd Int. Conf. Electr. Mach. Syst. (ICEMS)*, Aug. 2019, pp. 1–5, doi: [10.1109/ICEMS.2019.8922115](https://doi.org/10.1109/ICEMS.2019.8922115).
- [11] A. Nekoubin, "Design a single-phase BLDC motor and finite-element analysis of stator slots structure effects on the efficiency," *Int. J. Electr. Comput. Eng.*, vol. 5, no. 5, pp. 685–692, 2011.
- [12] Y. Park, J. Cho, and D. Kim, "Cogging torque reduction of single-phase brushless DC motor with a tapered air-gap using optimizing notch size and position," *IEEE Trans. Ind. Appl.*, vol. 51, no. 6, pp. 4455–4463, Nov. 2015, doi: [10.1109/TIA.2015.2453131](https://doi.org/10.1109/TIA.2015.2453131).
- [13] Z. Tang, Y. Chen, H. Hsu, R. Liang, and C. Hung, "An initial states recognition (ISR) method for start-up of 1 $\Phi$  BLDC motor in hall-sensor-less fan applications," *IEEE Trans. Ind. Electron.*, vol. 67, no. 10, pp. 8302–8311, Oct. 2020, doi: [10.1109/TIE.2019.2947849](https://doi.org/10.1109/TIE.2019.2947849).
- [14] Z. You and S. Yang, "Control system for a single-phase DC-excited flux-switching machine with a torque ripple reduction scheme," *IEEE Access*, vol. 8, pp. 226579–226590, 2020, doi: [10.1109/ACCESS.2020.3045390](https://doi.org/10.1109/ACCESS.2020.3045390).
- [15] Z. Q. Zhu, "Control of single-phase permanent magnet brushless DC drives for high-speed applications," in *Proc. 8th Int. Conf. Power Electron. Variable Speed Drives*, 2000, pp. 327–332, doi: [10.1049/cp:20000267](https://doi.org/10.1049/cp:20000267).
- [16] L. Schwager, A. Tüysüz, C. Zwyssig, and J. W. Kolar, "Modeling and comparison of machine and converter losses for PWM and PAM in high-speed drives," *IEEE Trans. Ind. Appl.*, vol. 50, no. 2, pp. 995–1006, Mar. 2014, doi: [10.1109/TIA.2013.2272711](https://doi.org/10.1109/TIA.2013.2272711).
- [17] C. Cui, G. Liu, and K. Wang, "A novel drive method for high-speed brushless DC motor operating in a wide range," *IEEE Trans. Power Electron.*, vol. 30, no. 9, pp. 4998–5008, Sep. 2015, doi: [10.1109/TPEL.2014.2361752](https://doi.org/10.1109/TPEL.2014.2361752).
- [18] Z.-H. Tang, Y.-T. Chen, C.-L. Chiu, and R.-H. Liang, "An indirect current phase detection method applied to automatic phase compensation driver for 1 $\Phi$  BLDC fan motor," *Electr. Power Compon. Syst.*, vol. 46, nos. 11–12, pp. 1340–1350, Jul. 2018, doi: [10.1080/15325008.2018.1488893](https://doi.org/10.1080/15325008.2018.1488893).
- [19] W. Lee, J. H. Kim, W. Choi, and B. Sarlioglu, "Torque ripple minimization control technique of high-speed single-phase brushless DC motor for electric turbocharger," *IEEE Trans. Veh. Technol.*, vol. 67, no. 11, pp. 10357–10365, Nov. 2018, doi: [10.1109/TVT.2018.2866779](https://doi.org/10.1109/TVT.2018.2866779).
- [20] S. Xia, S. Wang, and D. Bi, "Control performance of high-speed single-phase brushless DC motors," in *Proc. 22nd Int. Conf. Electr. Mach. Syst. (ICEMS)*, Aug. 2019, pp. 1–6, doi: [10.1109/ICEMS.2019.8921698](https://doi.org/10.1109/ICEMS.2019.8921698).
- [21] S. P. S. Rajawat, U. K. Kalla, and S. Singh, "A comprehensive study on torque ripple reduction in sensorless PMLDCM drive," in *Proc. Int. Conf. Sustain. Energy Future Electric Transp. (SEFET)*, Jan. 2021, pp. 1–6, doi: [10.1109/SeFet48154.2021.9375775](https://doi.org/10.1109/SeFet48154.2021.9375775).
- [22] O. Ammari, K. E. Majdoub, R. Baz, and A. Taouni, "Longitudinal modelling of electric vehicle driven by a BLDC in-wheel motor based on pacejka tire model," in *Proc. Int. Conf. Electr., Commun., Comput. Eng. (ICECCE)*, Jun. 2021, pp. 1–6, doi: [10.1109/ICECCE52056.2021.9514238](https://doi.org/10.1109/ICECCE52056.2021.9514238).
- [23] M. Mahmud, S. M. A. Motakabber, A. H. M. Z. Alam, and A. N. Nordin, "Adaptive PID controller using for speed control of the BLDC motor," in *Proc. IEEE Int. Conf. Semiconductor Electron. (ICSE)*, Jul. 2020, pp. 168–171, doi: [10.1109/ICSE49846.2020.9166883](https://doi.org/10.1109/ICSE49846.2020.9166883).
- [24] C. Chu, Y. Wang, and H. Liang, "SISO PID-fuzzy controller for BLDC motor speed control base on low cost MSP430 solution," in *Proc. 5th Int. Symp. Next-Gener. Electron. (ISNE)*, May 2016, pp. 1–2, doi: [10.1109/ISNE.2016.7543331](https://doi.org/10.1109/ISNE.2016.7543331).
- [25] J. Knobloch, J. Cibor, and P. Vorel, "Hardware concept of a new BLDC motor controller based on BCD technology," in *Proc. Int. Conf. Electr. Drives Power Electron. (EDPE)*, Sep. 2019, pp. 217–220, doi: [10.1109/EDPE.2019.8883916](https://doi.org/10.1109/EDPE.2019.8883916).
- [26] K. Guo, M. Yang, X. Li, P. Shi, and P. Wang, "Research on a new adaptive integral sliding mode controller based on a small BLDC," *IEEE Access*, vol. 10, pp. 73204–73213, 2022, doi: [10.1109/ACCESS.2022.3188665](https://doi.org/10.1109/ACCESS.2022.3188665).
- [27] J. Torres, D. Chavez, H. Aboukheir, M. Herrera, J. Prado, and O. Camacho, "Anti-windup algorithms for sliding mode control in processes with variable dead-time," in *Proc. IEEE ANDESCON*, Oct. 2020, pp. 1–6, doi: [10.1109/ANDESCON50619.2020.9272092](https://doi.org/10.1109/ANDESCON50619.2020.9272092).
- [28] H. Masoudi, A. Kiyomarsi, S. M. Madani, and M. Ataei, "Torque ripple reduction of non-sinusoidal brushless DC motor based on super-twisting sliding mode direct power control," *IEEE Trans. Transport. Electric.*, early access, Mar. 1, 2023, doi: [10.1109/TTE.2023.3250950](https://doi.org/10.1109/TTE.2023.3250950).
- [29] A. Rubaai and P. Young, "Hardware/software implementation of fuzzy-neural-network self-learning control methods for brushless DC motor drives," *IEEE Trans. Ind. Appl.*, vol. 52, no. 1, pp. 414–424, Jan. 2016, doi: [10.1109/TIA.2015.2468191](https://doi.org/10.1109/TIA.2015.2468191).
- [30] A. Sedaghati, N. Pariz, M. Siah, and R. Barzamani, "A new fuzzy control system based on the adaptive immersion and invariance control for brushless DC motors," *Int. J. Dyn. Control*, vol. 9, no. 2, pp. 807–817, Jun. 2021, doi: [10.1007/s40435-020-00663-6](https://doi.org/10.1007/s40435-020-00663-6).
- [31] S. Wongkhead, "State space model for speed control BLDC motor tuning by combination of PI-artificial neural network controller," in *Proc. 18th Int. Conf. Electr. Eng./Electron., Comput., Telecommun. Inf. Technol. (ECTI-CON)*, May 2021, pp. 874–877, doi: [10.1109/ECTI-CON51831.2021.9454756](https://doi.org/10.1109/ECTI-CON51831.2021.9454756).

- [32] S. Arandhakar, A. Kant, and M. N. Bhukya, "Implementation of convolutional neural network for speed control of BLDC motor," in *Proc. Int. Conf. Design Innov. 3Cs Compute Communicate Control (ICDIC)*, Jun. 2021, pp. 35–40, doi: [10.1109/ICDI3C53598.2021.00016](https://doi.org/10.1109/ICDI3C53598.2021.00016).
- [33] R. Busetto, A. Lucchini, S. Formentin, and S. M. Savaresi, "Data-driven optimal tuning of BLDC motors with safety constraints: A set membership approach," *IEEE/ASME Trans. Mechatronics*, early access, May 9, 2023, doi: [10.1109/TMECH.2023.3269515](https://doi.org/10.1109/TMECH.2023.3269515).
- [34] M. Fazil and K. R. Rajagopal, "Nonlinear dynamic modeling of a single-phase permanent-magnet brushless DC motor using 2-D static finite-element results," *IEEE Trans. Magn.*, vol. 47, no. 4, pp. 781–786, Apr. 2011, doi: [10.1109/TMAG.2010.2103955](https://doi.org/10.1109/TMAG.2010.2103955).
- [35] S. Shastri, U. Sharma, and B. Singh, "Design and analysis of Halbach array assisted PM brushless DC motor for ceiling fan," in *Proc. IEEE Int. Conf. Power Electron., Smart Grid Renew. Energy (PESGRE)*, Jan. 2020, pp. 1–6, doi: [10.1109/PESGRE45664.2020.9070686](https://doi.org/10.1109/PESGRE45664.2020.9070686).
- [36] P. C. Krause, O. Wasynczuk, S. D. Sudhoff, and S. D. Pekarek, *Analysis of Electric Machinery and Drive Systems*, vol. 75. Hoboken, NJ, USA: Wiley, 2013.
- [37] C.-H. Hsu and C.-W. Chang, "Permanent magnetic brushless DC motor magnetism performance depends on different intelligent controller response," *Trans. Can. Soc. Mech. Eng.*, vol. 45, no. 2, pp. 287–296, Jun. 2021, doi: [10.1139/tcsme-2020-0058](https://doi.org/10.1139/tcsme-2020-0058).
- [38] A. E. Fitzgerald, C. Kingsley, and S. D. Umans, *Electric Machinery*, 6th ed. McGraw-Hill, Jan. 2005.
- [39] S. Khader, "Single phase brushless DC motor with PWM control strategy and special form of PM rotor," *Jordan J. Appl. Sci. Nat. Sci.*, vol. 9, no. 2, p. 171, 2007.
- [40] J. Pongfai and W. Assawinchaichote, "Optimal PID parametric auto-adjustment for BLDC motor control systems based on artificial intelligence," in *Proc. Int. Electr. Eng. Congr. (IEECON)*, Mar. 2017, pp. 1–4, doi: [10.1109/IEECON.2017.8075892](https://doi.org/10.1109/IEECON.2017.8075892).
- [41] V. Samavatian and A. Radan, "A high efficiency input/output magnetically coupled interleaved buck–boost converter with low internal oscillation for fuel-cell applications: Small signal modeling and dynamic analysis," *Int. J. Electr. Power Energy Syst.*, vol. 67, pp. 261–271, May 2015, doi: [10.1016/j.ijepes.2014.11.011](https://doi.org/10.1016/j.ijepes.2014.11.011).
- [42] V. Samavatian and A. Radan, "A high efficiency input/output magnetically coupled interleaved buck–boost converter with low internal oscillation for fuel-cell applications: CCM steady-state analysis," *IEEE Trans. Ind. Electron.*, vol. 62, no. 9, pp. 5560–5568, Sep. 2015, doi: [10.1109/TIE.2015.2408560](https://doi.org/10.1109/TIE.2015.2408560).
- [43] O. S. Ebrahim and P. K. Jain, "LQR-based stator field oriented control for the induction motor drives," in *Proc. 23rd Annu. IEEE Appl. Power Electron. Conf. Expo.*, Feb. 2008, pp. 1126–1131, doi: [10.1109/APEC.2008.4522863](https://doi.org/10.1109/APEC.2008.4522863).
- [44] F. W. Fairman, *Linear Control Theory: The State Space Approach*. Hoboken, NJ, USA: Wiley, 1998.
- [45] S. Bittanti, A. J. Laub, and J. C. Willems, *The Riccati Equation*. Berlin, Germany: Springer, Dec. 2012.
- [46] Z. Tang and P. A. Fishwick, "Feedforward neural nets as models for time series forecasting," *ORSA J. Comput.*, vol. 5, no. 4, pp. 374–385, Nov. 1993.
- [47] A. P. Dempster, N. M. Laird, and D. B. Rubin, "Maximum likelihood from incomplete data via the EM algorithm," *J. Roy. Stat. Soc. B*, vol. 39, no. 1, pp. 1–22, Sep. 1977.
- [48] P. Mishra, A. Banerjee, M. Ghosh, S. Gogoi, and R. Dutta, "Development of a cost-effective circuit hardware architecture for brushless direct current motor driver," *Int. J. Circuit Theory Appl.*, vol. 49, no. 7, pp. 2183–2198, Jul. 2021, doi: [10.1002/cta.3011](https://doi.org/10.1002/cta.3011).



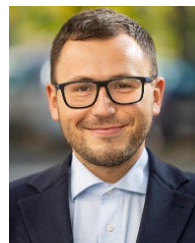
directions. The current research related products include robot balance systems.

**YANG ZHANG** was born in Shijiazhuang, Hebei, China. He received the master's degree in software engineering from Beihang University, in 2010. He is currently with Beijing Aiqi Technology Company Ltd. The robot four-wheel control systems has formed corresponding application products. He holds 200 patents and 30 invention patents. His research interests include intelligent robot, robot operating systems, robot control systems, robot programming systems, and other directions. The current research related products include robot balance systems.



reliability, the optimization of maintenance, and renewable energy sources.

**RADOMIR GONO** (Senior Member, IEEE) received the M.Sc., Ph.D., and Habilitate Doctorate degrees in electrical power engineering, in 1995, 2000, and 2008, respectively. In 2019, he was a Professor of electrical power engineering. Since 1999, he has been with the Department of Electrical Power Engineering, VSB—Technical University of Ostrava, Czech Republic, where he is currently a Professor and the Vice-Head. His research interests include electric power systems



quality and optimization in multicarrier energy systems. He is the Guest Editor of Special Issues in *Energies*, *Electronics*, *Sustainability*, and *Frontiers in Energy Research*.

**MICHAŁ JASIŃSKI** (Member, IEEE) received the M.S. and Ph.D. degrees in electrical engineering from the Wrocław University of Science and Technology, in 2016 and 2019, respectively. Since 2018, he has been with the Faculty of Electrical Engineering, Wrocław University of Technology, where he is currently an Assistant Professor. He is the author and coauthor of more than 100 scientific publications. His research interest include big data in power systems, especially in point of power

• • •